ETH
Eidgenössische Technische Hochschule Zürich
Swiss Federal Institute of Technology Zurich

Seminar for Applied Mathematics SAM

Fourier Spectral Dynamic Data Assimilation: Interlacing CFD with 4D Flow MRI

T. S. Koltukluoglu

Research Report No. 2019-56
September 2019

Seminar für Angewandte Mathematik
Eidgenössische Technische Hochschule
CH-8092 Zürich
Switzerland

Fourier Spectral Dynamic Data Assimilation: Interlacing CFD with 4D Flow MRI

Taha Sabri Koltukluoğlu

Seminar for Applied Mathematics, ETH, Zurich, CH
ktaha@ethz.ch

Abstract. Most data assimilation studies, incorporating observations into computational blood flow simulations, have approached the problem exploiting the traditional mathematical formulation in the time domain, an approach that incurs huge computational cost. In this work, a new method is introduced to perform variational adjoint-based dynamic data assimilation. The work aims to combine the superiority of computational fluid dynamics with the advantages of phase-contrast magnetic resonance imaging and simultaneously taking into account the dynamic nature of the heart beat. In contrast to the traditional time-stepping schemes, the novel approach relies on the harmonically balanced momentum equations expressed in the frequency domain, while the combination of the corresponding solutions yields the periodic solution of the original problem. This work enables accurate characterization of the dynamic flow field in quite feasible and practicable wall clock times, which are otherwise difficult to be achieved using currently available dynamic data assimilation strategies.

1 Introduction

In time dependent adjoint-based inverse problems, all trajectories of the state variables from the original problem must be solved and stored in the memory, in order to solve the adjoint equations. The space needed for the memory is proportional to the run-time of the forward solution. In spite of ever increasing memory capabilities of large clusters, the practical application of the traditional adjoint formulation is quite limited. Certain algorithms, known as checkpointing, have been proposed to manage the difficulties with the storage requirements [3, 8, 1]. When using such algorithms, however, the direct problem must be solved several times in order to evaluate the adjoint problem. This process must then be repeated at each single iteration of the optimization process.

There has been an attempt to perform variational adjoint-based dynamic data assimilation (DA) in computational hemodynamics [2]. However, the authors were forced to extremely reduce the size of the problem (in such a way, that no checkpointing algorithms were required) by considering a coarse mesh and a time step of 0.004625 s. Using such time steps, however, accurate flow simulations cannot be expected at the aortic root and the ascending aorta, where the Reynolds numbers grow large. In addition, finer mesh sizes are required

for reasonable evaluation of clinically relevant parameters such as the wall shear stresses (WSSs). The size-related limitations were also mentioned by the authors in their work. Especially for convection dominated problems with large Reynolds numbers, using the traditional time-stepping schemes to perform dynamic DA is absolutely impracticable and nearly impossible or difficult to be achieved.

In this work, a new method is proposed to perform variational adjoint-based dynamic data assimilation. In contrast to the traditional time-stepping schemes, the novel approach relies on the harmonically balanced momentum equations (see [6]) for the time discretization, which are expressed in the frequency domain. The combination of the corresponding solutions in the frequency domain yields the periodic solution of the original problem. Hereinafter, the new method will be referred as the Fourier spectral dynamic data assimilation (FS-DDA). This work enables accurate characterization of the dynamic flow field in quite feasible and practicable wall clock times (WCT), which are otherwise difficult or impossible to be achieved using currently available DA strategies. The method naturally avoids storage related problems, and hence, the application of additional algorithms (such as checkpointing) are not required. Further, the work addresses the limited resolution of MR velocity encoding in shear layers and aims to interlace phase-contrast magnetic resonance imaging (4D flow MRI) with computational fluid dynamics (CFD) to enable the evaluation of clinically relevant parameters. Compared to the raw measurements, the proposed approach significantly improves the reconstructed flow field at the aortic root, which is one of the most important clinically relevant locations where flow disturbances can easily lead to pathological modifications of the arterial wall. Thus the new method has a great potential for revealing clinically relevant hemodynamic phenomena.

2 Mathematical Optimization

An unsteady incompressible flow of a Newtonian fluid is considered in the time interval $\mathbb{T} := [0;T]$ through an open set Ω with boundary $\partial\Omega = \Gamma_i \cup \Gamma_o \cup \Gamma_w$. Let $\Omega \supset \Omega_s := \{\, x \in \Omega \mid \|x-y\| \geq s\,(\mathrm{mm})\ \forall y \in \Gamma_w \,\}$ be a contracted subdomain with boundary $\partial\Omega_s = \Gamma_{si} \cup \Gamma_{so} \cup \Gamma_{sw}$, where $\Gamma_{si} \subset \Gamma_i$ and $\Gamma_{so} \subset \Gamma_o$ (see Figure 1). The fluid flow is stimulated by some T-periodic inflow data prescribed at Γ_i, which is characterized by the T-periodic function $g(t,x) = g(t+mT,x) : \mathbb{T}\times\Gamma_i \to \mathbb{R}^3$ with $m \in \mathbb{N}$. Let $H^1(\Omega)$ be the space of square integrable vector functions with first derivatives also square integrable in Ω, whereas $L^2(\Omega)$ is the space of square integrable scalar functions in Ω. The blood flow velocity $u \in \mathcal{U}$ with $\mathcal{U} = \left\{\, v \in H^1(\Omega) \mid v|_{\Gamma_w} = \mathbf{0} \,\right\}$ is a solution of the incompressible Navier-Stokes equations, which can be expressed in the Euler-Lagrangian formulation as a set of equations for momentum $\rho\,[\,\partial_t u + (\nabla u)u\,] - \mu\Delta u + \nabla p = \mathbf{0}$ and continuity $\operatorname{div} u = 0$ in $\mathbb{T}\times\Omega$ (along with inflow $u = g$ on $\mathbb{T}\times\Gamma_i$), where $p \in L^2(\Omega)$ and (ρ,μ) are the density and dynamic viscosity of the fluid.

In [6], the harmonic balance (HB) approach has been employed for an approximation of the velocity field in time, which relies on the degree-n Fourier polynomial $u \approx \tilde{u}(t,x) = \hat{u}_{c_0}(x) + \sum_{k=1}^{n} \left[\hat{u}_{c_k}(x)\cos(k\omega t) + \hat{u}_{s_k}(x)\sin(k\omega t)\right]$, where

$\hat{u}_{c_k}$ for $k = 0 \cdots n$ and $\hat{u}_{s_k}$ for $k = 1 \cdots n$ form the discrete spectrum of $\tilde{u}$ and $\omega = \frac{2\pi}{T}$ is the angular frequency. Let $\tilde{u}^j := \tilde{u}(t_j, x)$ and $p^j := p(t_j, x)$. Inserting the approximation $\tilde{u}$ into the momentum equation and employing a collocation approach using equidistant time instants $t_j := \frac{jT}{N}$ for $j = 1, \cdots, N = 2n + 1$ results in the following harmonically balanced momentum equations,

$$\rho\Big[\sum_{i=1}^{N} \tilde{u}^{\,i} c_{ij} + (\nabla \tilde{u}^{\,j})\tilde{u}^{\,j}\Big] - \mu\Delta\tilde{u}^{\,j} + \nabla p^j = \mathbf{0}\,, \qquad j = 1, 2, \cdots, N. \tag{1}$$

The expression $c_{ij} = \frac{2\omega}{N}\sum_{k=1}^{n} k \sin(k\omega(t_i - t_j))$ follows from the application of cosine and sine transforms (DFT) for the discrete spectrum. Equations in (1) are expressed in the frequency domain in terms of the time domain state variables $\tilde{u}^{\,j}$ and p^j at each time t_j. Detailed derivations can be found in [6].

In this work, a new method is introduced by incorporating the harmonically balanced momentum equations (1) into an optimal boundary control study and performing a variational adjoint-based data assimilation using 4D flow MRI data. As such, let us first express the harmonically balanced incompressible Navier-Stokes equations in the variational formulation as follows: Find $(u, p, r) \in \mathcal{U} \times L^2(\Omega) \times H^{-\frac{1}{2}}(\Gamma_i)$ such that $\forall\, (\hat{u}^j, \hat{p}^j, \hat{r}^j) \in \mathcal{U} \times L^2(\Omega) \times H^{-\frac{1}{2}}(\Gamma_i)$ it holds

$$\begin{aligned}
&\int_\Omega \left[\rho\Big(\sum_{i=1}^{N} \tilde{u}^{\,i} c_{ij} + (\nabla u^j)u^j\Big)\cdot \hat{u}^j + 2\mu\nabla^s u^j : \nabla^s \hat{u}^j - p^j \operatorname{div} \hat{u}^j - \hat{p}^j \operatorname{div} u^j\right] d\Omega \\
&= \int_{\Gamma_i} \hat{r}^j \cdot (u^j - g^j)\, d\Gamma + \int_{\Gamma_i} (r^j \cdot \hat{u}^j)\, d\Gamma \;, \quad j = 1, 2, \cdots, N \;,
\end{aligned} \tag{2}$$

where $\nabla^s(\cdot) = [\nabla(\cdot) + (\nabla(\cdot))^T]/2$ is the strain rate tensor and $H^{-\frac{1}{2}}(\Gamma_i)$ is the dual space of $H^{\frac{1}{2}}_{00}(\Gamma_i) = \Big\{\, g \in H^{\frac{1}{2}}(\Gamma_i) \;\mid\; g|_{\gamma_i} = 0 \,\Big\}$.

Assuming that some T-periodic observations $u^j_{\mathbf{obs}} \in \Omega$ are available at equidistantly spaced discrete time instants t_j. The optimal control problem aims at finding the velocity fields u^j, such that the sum of the misfits between each $u^j_{\mathbf{obs}}$ and u^j is minimized based on some cost function $\mathscr{O}_\Omega$. At the same time, the problem is constrained such that u^j are solutions of equation (2). Let β and β_1 be arbitrary parameters for a Tikhonov regularization, whereas ∇_τ denotes the surface gradient and α is a positive real number. The flow-matching problem reads $\mathscr{O}_\Omega(u(g), g, u_{\mathbf{obs}}) = \frac{\alpha}{2}\sum_j \Big(\int_{\Omega_s} |u^j(g) - u^j_{\mathbf{obs}}|^2\, d\Omega + \int_{\Gamma_{si}\cup\Gamma_{so}} |u^j(g) - u^j_{\mathbf{obs}}|^2\, d\Gamma\Big) + \sum_j \Big(\frac{\beta}{2}\int_{\Gamma_i} |g^j|^2\, d\Gamma + \frac{\beta_1}{2}\int_{\Gamma_i} |\nabla_\tau\, g^j|^2\, d\Gamma\Big)$, where Ω_s, Γ_{si} and Γ_{so} are the trust regions of experimental observations (see Figure 1). The terms with the regularization parameters prevent the control function to grow unboundedly and enforce a certain regularity over the control. The choices of these terms were also motivated in [5]. Further, the choices of the terms for performing the flow-matching both in a part of the domain (in Ω_s) and in parts over the boundaries (on Γ_{si} and Γ_{so}) has been investigated in [7]. Regarding the flow-matching problem, the existence of optimal boundary control has been provided in [4].

The constrained optimization can be cast as a saddle point problem by introducing a Lagrangian functional: $\mathscr{L}_\Omega(g,u,p,r,\lambda_u,\lambda_p,\lambda_r) = \mathscr{O}_\Omega(u,g,u_{\mathbf{obs}}) - \sum_j \int_{\Gamma_i} \lambda_r^j \cdot (u^j - g^j)\, d\Gamma - \sum_j \int_{\Gamma_i} r^j \cdot \lambda_u^j \, d\Gamma + \sum_j \int_\Omega \big[\rho(\sum_{i=1}^N u^i c_{ij} + (\nabla u^j)u^j)\cdot\lambda_u^j + 2\mu\nabla^s u^j \cdot \nabla^s \lambda_u^j - p^j \operatorname{div}\lambda_u^j - \lambda_p^j \operatorname{div} u^j\big]\, d\Omega$. The necessary condition for having a minimum at g is provided by the Gâteaux derivative of $\mathscr{O}_\Omega$ with respect to perturbation in g. This information is contained in the critical points of the Lagrangian $\mathscr{L}_\Omega$, expressed in variational formulation for $j = 1 \cdots N$ as follows:

Direct Problem $\mathscr{P}^j_{\mathbf{sta}}(g^j, u^i)$: For $g^j \in H^{\frac{1}{2}}_{00}(\Gamma_i)$ and $u^i \in \mathcal{U}$, where $i = 1, \cdots, N$ with $i \neq j$, determine $(u^j, p^j, r^j) \in \mathcal{U} \times L^2(\Omega) \times H^{-\frac{1}{2}}(\Gamma_i)$ such that

$$\left\langle \frac{\partial \mathscr{L}_\Omega}{\partial \lambda_u^j}, \hat{\lambda}_u^j \right\rangle = \int_\Omega \Big[\rho\Big(\sum_{i=1}^N u^i c_{ij} + (\nabla u^j)u^j\Big)\cdot\hat{\lambda}_u^j + 2\mu\nabla^s u^j \cdot \nabla^s \hat{\lambda}_u^j - p^j \operatorname{div}\hat{\lambda}_u^j\Big]\, d\Omega - \int_{\Gamma_i} r^j \cdot \hat{\lambda}_u^j \, d\Gamma = 0 \qquad \forall\, \hat{\lambda}_u^j \in \mathcal{U} \ , \tag{3}$$

$$\left\langle \frac{\partial \mathscr{L}_\Omega}{\partial \lambda_p^j}, \hat{\lambda}_p^j \right\rangle = -\int_\Omega \hat{\lambda}_p^j \operatorname{div} u^j \, d\Omega = 0 \qquad \forall\, \hat{\lambda}_p^j \in L^2(\Omega) \ , \tag{4}$$

$$\left\langle \frac{\partial \mathscr{L}_\Omega}{\partial \lambda_r^j}, \hat{\lambda}_r^j \right\rangle = -\int_{\Gamma_i} \hat{\lambda}_r^j \cdot (u^j - g^j)\, d\Gamma = 0 \qquad \forall\, \hat{\lambda}_r^j \in H^{-\frac{1}{2}}(\Gamma_i) \ . \tag{5}$$

Adjoint Problem $\mathscr{P}^j_{\mathbf{adj}}(u^j, u^j_{\mathbf{obs}})$: For u^j, solution of (3)–(5), and $u^j_{\mathbf{obs}}$, determine $(\lambda_u^j, \lambda_p^j, \lambda_r^j) \in \mathcal{U} \times L^2(\Omega) \times H^{-\frac{1}{2}}(\Gamma_i)$ such that

$$\left\langle \frac{\partial \mathscr{L}_\Omega}{\partial u^j}, \hat{u}^j \right\rangle = \int_{\Gamma_o \cup \Gamma_i} \Big[\alpha\,(\chi_{\Gamma_{so}} + \chi_{\Gamma_{si}})(u^j - u^j_{\mathbf{obs}})\cdot\hat{u}^j\Big]\, d\Gamma - \int_{\Gamma_i} (\lambda_r^j \cdot \hat{u}^j)\, d\Gamma + \int_\Omega \Big[\alpha\,\chi_{\Omega_s}(u^j - u^j_{\mathbf{obs}})\cdot\hat{u}^j + \rho\Big(\sum_{i=1}^N c_{ji}\hat{u}^j + (\nabla\hat{u}^j)u^j + (\nabla u^j)\hat{u}^j\Big)\cdot\lambda_u^j + 2\mu\nabla^s\hat{u}^j \cdot \nabla^s\lambda_u^j - \lambda_p^j \operatorname{div}\hat{u}^j\Big]\, d\Omega = 0 \qquad \forall\, \hat{u}^j \in \mathcal{U} \ , \tag{6}$$

$$\left\langle \frac{\partial \mathscr{L}_\Omega}{\partial p^j}, \hat{p}^j \right\rangle = -\int_\Omega \hat{p}^j \operatorname{div}\lambda_u^j \, d\Omega = 0 \qquad \forall\, \hat{p}^j \in L^2(\Omega) \ , \tag{7}$$

$$\left\langle \frac{\partial \mathscr{L}_\Omega}{\partial r^j}, \hat{r}^j \right\rangle = -\int_{\Gamma_i} \hat{r}^j \cdot \lambda_u^j \, d\Gamma = 0 \qquad \forall\, \hat{r}^j \in H^{-\frac{1}{2}}(\Gamma_i) \ , \tag{8}$$

where χ_{Ω_s}, $\chi_{\Gamma_{si}}$ and $\chi_{\Gamma_{so}}$ are the characteristic functions.

Optimality Condition $\mathscr{P}^j_{\mathbf{opt}}(\lambda_r^j)$: For λ_r^j, solution of (6)–(8), determine $g^j \in H^{\frac{1}{2}}_{00}(\Gamma_i)$ such that $\forall\, \hat{g}^j \in H^{\frac{1}{2}}(\Gamma_i)$ it holds

$$\left\langle \frac{\partial \mathscr{L}_\Omega}{\partial g^j}, \hat{g}^j \right\rangle = \int_{\Gamma_i} \Big[\beta g^j \cdot \hat{g}^j + \beta_1 \nabla_\tau g^j \cdot \nabla_\tau \hat{g}^j + \lambda_r^j \cdot \hat{g}^j\Big]\, d\Gamma = 0 \ . \tag{9}$$

2.1 Gradient Descent Algorithm for Dynamic Data Assimilation

A descent-like iterative algorithm was employed to iteratively solve the nonlinear system of coupled variational equations $\mathscr{P}^j_{\text{sta}}$, $\mathscr{P}^j_{\text{adj}}$ and $\mathscr{P}^j_{\text{opt}}$. This procedure is described in algorithm 1. The fields $(\cdot)^{\{k\}}$ correspond to the fields $(\cdot)$ at the k-th iteration. The parameters σ^j, being adjusted dynamically, represent the step sizes for the j-th HB iteration of each optimization procedure. A tolerance parameter ξ is prescribed to test for convergence and exit the algorithm, if necessary. Spatial discretization of the equations described in the present section and the numerical methods applied to solve the aforementioned problems are as presented in [6].

Algorithm 1 Multiple steepest descent optimization with dynamic step sizes

Input : $\alpha, \beta, \beta_1 > 0$, n ▷ Optimization parameters and harmonics n
$(u^j)^{\{0\}}, (g^j)^{\{0\}}, (p^j)^{\{0\}}, u^j_{\mathbf{obs}}$ ▷ Initial guesses $(\cdot)^{\{0\}}$ and target fields
Output : $(u^j)^{\{k\}},\ (p^j)^{\{k\}}$ ▷ Flow fields at last iteration k

procedure DynamicDataAssimilation($u^{\{0\}}, g^{\{0\}}, u_{\mathbf{obs}}, N$)
  $\xi \leftarrow 10^{-8}$, $k \leftarrow 0$ and $\sigma^j \leftarrow 1$ for $j = 1, 2, \cdots, N$
  for $j \leftarrow 1, N$ **do**
    $((u^j)^{\{k\}}, \cdot, \cdot) \leftarrow \mathscr{P}^j_{\text{sta-lin}}((u^j)^{\{0\}}, (g^j)^{\{0\}}, u^i)$ ▷ Evaluate (3)–(5)
    update u^i using new $(u^j)^{\{k\}}$ for $i = j$
  $cost^{\{k\}} \leftarrow \mathscr{O}_\Omega(u^{\{k\}}, g^{\{0\}}, u_{\mathbf{obs}})$ ▷ Evaluate cost function $\mathscr{O}_\Omega$
  for $k \leftarrow 1, \infty$ **do**
    $converged \leftarrow$ **true**
    for $j \leftarrow 1, N$ **do**
      $(\cdot, \cdot, (\lambda^j_r)^{\{k\}}) \leftarrow \mathscr{P}^j_{\text{adj}}((u^j)^{\{k-1\}}, u^j_{\mathbf{obs}})$ ▷ Evaluate (6)–(8)
      $(s^j)^{\{k\}} \leftarrow \beta_1 \triangle_\tau (g^j)^{\{k-1\}} - \beta (g^j)^{\{k-1\}} - (\lambda^j_r)^{\{k\}}$ ▷ Steepest descent
      repeat
        $(g^j)^{\{k\}} \leftarrow (g^j)^{\{k-1\}} + \sigma^j (s^j)^{\{k\}}$ ▷ Update control using σ^j
        $((u^j)^{\{k\}}, \cdot, \cdot) \leftarrow \mathscr{P}^j_{\text{sta-lin}}((u^j)^{\{k-1\}}, (g^j)^{\{k\}}, u^i)$
        $cost^{\{k\}} \leftarrow \mathscr{O}_{\mathbb{T}}(u^{\{k\}}, g^{\{k\}}, u_{\mathbf{obs}})$
        if $cost^{\{k\}} \geq cost^{\{k-1\}}$ **then** $\sigma^j \leftarrow 0.5\sigma^j$
      until $cost^{\{k\}} < cost^{\{k-1\}}$
      if $(\left|cost^{\{k\}} - cost^{\{k-1\}}\right|)/(cost^{\{k\}}) > \xi$ **then**
        $\sigma^j \leftarrow 1.5\sigma^j$ & $converged \leftarrow$ **false**
      update u^i using new $(u^j)^{\{k\}}$ for $i = j$
    if $(converged)$ **then return** $(u^j)^{\{k\}},\ (p^j)^{\{k\}}$ for $j = 1 \cdots N$

3 Validation

Numerical computations are performed using computational mesh geometries denoted as $\mathbf{M_2}$, $\mathbf{M_4}$ and $\mathbf{M_7}$, with different numbers of cells, 215 000, 440 000 and 750 000 respectively. The mesh $\mathbf{M_7}$ will be referred to as the world domain, whereas the meshes $\mathbf{M_2}$ and $\mathbf{M_4}$ represent the MRI and CFD domains respectively. In the present section, a reference solution was numerically generated in the world domain $\mathbf{M_7}$, as described in [6], to serve as the ground truth for validation purposes. To test the proposed FS-DDA approach, $n = 12$ number of modes were considered, at which the HB treatment has proven to be satisfactorily accurate [6]. First, the reference solution in the world domain (mesh $\mathbf{M_7}$) was sampled at $N = 2n+1 = 25$ equidistantly placed time instants and the samples were mapped into the MRI domain (mesh $\mathbf{M_2}$) using linear interpolation. Second, an artificial noise with an isotropic VENC of 0.75 m/s and an SNR of 10 (see [7] for more details) was added to the flow fields in the MRI domain and the noisy samples were then mapped from $\mathbf{M_2}$ into the CFD domain $\mathbf{M_4}$, where the computational simulations were performed. Figure 1 illustrates these steps.

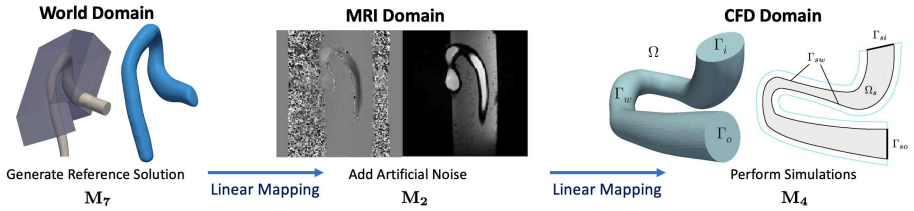

Fig. 1. Preparations for the validation of the proposed approach

Let $u_{\mathbf{snr}}$ denote the noisy field in $\mathbf{M_4}$. For FS-DDA, Algorithm 1 was executed with input parameters ($u^{\{0\}} = u_{\mathbf{snr}}$, $g^{\{0\}} = u_{\mathbf{snr}}$ on Γ_i, $u_{\mathbf{obs}} = u_{\mathbf{snr}}$, $N = 25$) resulting in the flow field $u_{\mathbf{hb}}^{\mathbf{opt}}$ (adopting HB into optimization). Flow matching was performed in Ω_2, a contracted domain at a distance of at least 2 mm from Γ_w. Optimization parameters α, β and β_1 were set to 1, 10^{-5} and 10^{-8} respectively. In addition, the HB method was employed as a forward simulation without adopting the assimilation process, resulting in the flow field $u_{\mathbf{hb}}$. Both computed fields are compared with a reference solution (ground truth data u_r) in terms of normalized root mean square error $\mathrm{nRMSE}^X(u_c, u_r) = \left(\frac{100}{\underset{\mathbb{T},X}{\mathrm{avr}}|u_r|}\right)\sqrt{\frac{1}{V_X \cdot T}\int_{\mathbb{T}}\int_X |u_c - u_r|^2\, dX\, dt}$, where X is a domain with volume V_X, and the flow direction error $\mathrm{FDE}^X(u_c, u_r) = \sqrt{\frac{1}{V_X \cdot T}\int_{\mathbb{T}}\int_X \left(1 - \frac{u_c \cdot u_r}{|u_c||u_r|}\right)^2 dX dt}$.

For the clinically relevant parameters, we are interested in the performance of the solvers at near-wall locations and in the close proximity of the inlet. Hence, for the evaluation of the errors nRMSE^X and FDE^X, we define the domain $X = E_2^4 \subset \Omega$, which is within 4cm proximity of the inlet and within a distance

of 2mm from the wall boundary. In addition, the errors were also evaluated in Ω. Under these conditions, the numerical results are as follows:

(x, y)	$\text{nRMSE}^{E_2^4}(x, y)$	$\text{FDE}^{E_2^4}(x, y)$	$\text{nRMSE}^{\Omega}(x, y)$	$\text{FDE}^{\Omega}(x, y)$
$(u_{\mathbf{snr}}, u_r)$	16.76%	0.367	6.90%	0.166
$(u_{\mathbf{hb}}, u_r)$	3.75%	0.095	1.66%	0.042
$(u_{\mathbf{hb}}^{\mathbf{opt}}, u_r)$	2.39%	0.055	1.59%	0.027

It can be observed that, compared with the results obtained from the HB method as a forward simulation, there is a significant improvement in the outcome provided by FS-DDA in the close proximity of the inlet. This is a remarkable finding for the improvement of the flow field, especially at the aortic root. The optimization process lasted for 54 iterations and the WCT was 943 seconds.

Dynamic Data Assimilation using 4D Flow MRI Acquisition For the optimal control problem, the proposed approach was tested in a realistic scenario using flow data gathered from real 4D flow MRI scans, as described in [6]. It is worth mentioning that the preprocessing steps detailed in [7], were also applied in the present section. This includes a projection of the observed flow field over a divergence-free space, which is useful in two ways. First, it recovers back the solenoidal property of the flow field, which is usually lost after the application of both the outlier detection scheme and the immediate mapping of the observations from MRI domain into the computational mesh domain (see [7]). Secondly, it allows to start the computations with a solenoidal initial guess.

Flow patterns obtained from both methods, FS-DDA and HB, were first compared with the MRI data by visual inspection. Figure 2 shows the magnitudes of the velocity fields, obtained from the noisy MRI measurements (in the middle) and from the computations using both the FS-DDA method (on the left) and the HB method (on the right) respectively. The presented slices correspond to the time instant at peak systole. One slice was placed at the aortic root and was oriented such that the velocity profiles in the close proximity of the inlet are clearly visible. Another slice was placed at the aortic arch to additionally illustrate the obtained flow patterns at a moderate distance from the inlet. It can be observed that the noise-free flow field obtained from the assimilation process is fairly close to the noisy flow field measured with 4D flow MRI, whereas the flow field obtained from a conventional forward simulation (without the optimization of the velocity components), is largely different compared to the measurements.

Since the observations are obtained from real 4D flow MRI acquisition, the obtained noisy flow field cannot be regarded as the ground truth. Therefore, the flow fields obtained from both methods were quantitatively compared with each other to demonstrate the extent of their difference from each other. In the whole domain, Ω, evaluation of the errors yielded $\text{nRMSE}^{\Omega}(u_{\mathbf{hb}}, u_{\mathbf{hb}}^{\mathbf{opt}}) = 21.66\%$ and $\text{FDE}^{\Omega}(u_{\mathbf{hb}}, u_{\mathbf{hb}}^{\mathbf{opt}}) = 0.229$, whereas in the close proximity of the inlet and at near-wall locations, the errors were $\text{nRMSE}^{E_2^4}(u_{\mathbf{hb}}, u_{\mathbf{hb}}^{\mathbf{opt}}) = 30.08\%$ and $\text{FDE}^{E_2^4}(u_{\mathbf{hb}}, u_{\mathbf{hb}}^{\mathbf{opt}}) = 0.314$. Notably, the better qualitative agreement between

the observations and the optimized solution, along with the quantitatively significant differences between the optimized solution and the predictions from conventional forwards CFD simulation, support the fact that the optimization delivers a better solution when compared with the conventional CFD approach.

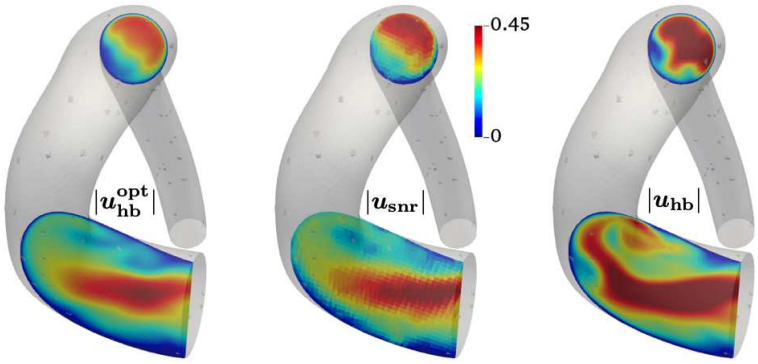

Fig. 2. Slices for the magnitudes of different velocity fields at the aortic root and arch.

4 Conclusion

This work has introduced the Fourier spectral dynamic data assimilation approach as a new method for an inverse problem to perform variational adjoint-based assimilation for pulsatile blood flow simulations. The method is being reported for the first time in computational hemodynamics and brings remarkable improvement in terms of computational effort without exhibiting deterioration of the approximate solution. This work enables accurate characterization of the dynamic flow field in quite feasible and practicable wall clock times, which are otherwise difficult or impossible to be achieved using currently available dynamic data assimilation strategies relying on traditional time-stepping schemes.

The proposed algorithm was examined in detail to estimate the efficiency of the methodology for reconstructing the blood flow at the aortic root and in near-wall regions. The new method proved to deliver physically consistent flow fields, with substantial reduction of noise present in the 4D flow MRI measurements, outperforming the predictive capabilities of conventional CFD approaches. The flow field is considerably improved at the aortic root, which is one of the most important clinically relevant locations for the development of pathological alterations of the anatomical structures underlying the arterial wall.

This work does not include the deformation of the arterial walls but is a starting point for the adaptation of contact modelling approaches for fluid-structure interaction studies. Hence, this investigation is the first of a series that will address the deformation and dynamic response of the arterial walls. The novel

approach provides a systematic strategy to improve the model predictions regarding clinically relevant hemodynamic data, such as the wall shear stresses, and reveals a great potential for clinical applicability.

References

1. Aupy, G., Herrmann, J.: Periodicity in optimal hierarchical checkpointing schemes for adjoint computations. Optim. Methods Softw. **32**(3), 594–624 (2017). https://doi.org/10.1080/10556788.2016.1230612
2. Funke, S.W., Nordaas, M., Evju, Ø., Alnæs, M.S., Mardal, K.A.: Variational data assimilation for transient blood flow simulations: Cerebral aneurysms as an illustrative example. Int. J. Numer. Method. Biomed. Eng. **35**(1), e3152 (2019). https://doi.org/10.1002/cnm.3152
3. Griewank, A., Walther, A.: Algorithm 799: Revolve: An implementation of checkpointing for the reverse or adjoint mode of computational differentiation. ACM Trans. Math. Softw. **26**(1), 19–45 (2000). https://doi.org/10.1145/347837.347846
4. Guerra, T., Sequeira, A., Tiago, J.: Existence of optimal boundary control for the navier–stokes equations with mixed boundary conditions. Port. Math. **72**(1), 267–283 (2015). https://doi.org/10.4171/PM/1968
5. Gunzburger, M.D., Manservisi, S.: The velocity tracking problem for navier–stokes flows with boundary control. SIAM J. Control Optim. **39**(2), 594–634 (2000). https://doi.org/10.1137/S0363012999353771
6. Koltukluoğlu, T.S.: Harmonic balance techniques in cardiovascular fluid mechanics. In: Shen, D., et al., T.L. (eds.) Med. Image. Comput. Comput. Assist. Interv. vol. ***, pp. ***–*** (2019). https://doi.org/********** ********** **********
7. Koltukluoğlu, T.S., Blanco, P.J.: Boundary control in computational haemodynamics. J. Fluid Mech. **847**, 329–364 (2018). https://doi.org/10.1017/jfm.2018.329
8. Wang, Q., Moin, P., Iaccarino, G.: Minimal repetition dynamic checkpointing algorithm for unsteady adjoint calculation. SIAM J. Sci. Comput. **31**(4), 2549–2567 (2009). https://doi.org/10.1137/080727890